

Irrotational flow analysis of Rayleigh-Taylor instability in nanofluid layer with tangential magnetic field

A. S. Rana^a, S. Gupta^b, S. K. Garg^c, V. Kumar^d, M. K. Awasthi^{e,*}

^aDepartment of Physics, Shri Guru Ram Rai (P.G.) College, Dehradun-248001, India

^bDepartment of Mathematics, Ismail National Mahila PG College, Meerut-250002, India

^cDepartment of Applied Science and Humanities, G. L. Bajaj Institute of Technology and Management, Greater Noida-201306, India

^dDepartment of Mathematics, Shri Guru Ram Rai (P.G.) College, Dehradun-248001, India

^eDepartment of Mathematics, Babasaheb Bhimrao Ambedkar University, Lucknow-226025, India

Received 26 August 2023; accepted 6 March 2024

Abstract

The application of nanofluids in the presence of a magnetic field holds promise for advanced drug delivery systems, where controlled manipulation of magnetic nanoparticles within nanofluids can enhance targeted and localized drug delivery. This study explores the instability of a viscous fluid-nanofluid interface arranged in a planar configuration influenced by a tangential magnetic field using the irrotational flow theory. When the nanofluid is positioned above a viscous fluid, the interface is susceptible to the Rayleigh-Taylor instability. Employing linear stability theory, an explicit relationship connecting the perturbation growth parameter with the wavenumber is derived. Different dimensionless quantities such as the Atwood number, Weber number, Froude number, and Reynolds number are analyzed using stability plots. These plots provide valuable information about the behavior of interfaces. Increased magnetic field strength is observed to delay instability onset. Surface tension is found to stabilize the interface, whereas inertial forces destabilize it. This investigation contributes to understanding and controlling the interface dynamics in nanofluid systems.

© 2024 University of West Bohemia.

Keywords: nanofluid, horizontal magnetic field, Rayleigh-Taylor instability, irrotational flow theory

1. Introduction

In [25], Rayleigh demonstrated that an equilibrium configuration of a fluid system, characterized by an uneven distribution of mass where the heavier fluid resides above the lighter fluid, becomes susceptible to gravitational destabilization. Taylor [29] later extended this finding to encompass accelerated fluid systems, wherein the heavier fluid situated atop the lighter fluid can lead to similar instability. This phenomenon is now termed the Rayleigh-Taylor instability (RTI). In the context of nuclear explosions, the vicinity of the detonation experiences a substantial rise in air temperature. The resulting hot air, encircled by the cooler ambient air, creates conditions favorable for the development of an unstable interface. Other instances of RTI include the formation of mushroom clouds and situations where water is suspended above oil, among others. In [17], Lewis made observations of RTI occurring at the interface between compressed gas and water. Emmons et al. [9] conducted experimental investigations on RTI, studying an accelerated interface between liquid and air and also considered the impact of surface tension. However, their efforts did not yield complete stabilization of the interface. In [5], Cole and Tankin replicated a similar experiment and achieved improved results in their findings.

*Corresponding author. Tel.: +91 993 564 74 45, e-mail: mukeshiitr.kumar@gmail.com.
<https://doi.org/10.24132/acm.2024.855>

Sharp [27] provided a comprehensive and detailed description of RTI. On the other hand, Jacobs and Catton [14] tackled the RTI problem in a three-dimensional configuration involving liquid and gas to arrive at a solution. Boffetta et al. [2] established intermittent statistics in RTI and demonstrated that the time-dependent behavior of the Reynolds and Nusselt numbers followed the Kraichnan scaling regime, which is associated with a highly pronounced level of thermal convection.

Particular emphasis has been placed on conducting experiments involving thin layers of ferrofluids, which have yielded a diverse array of structural configurations [3, 4, 7]. Ferrofluids are composite substances composed of magnetic nanoparticles dispersed within a colloidal solution. These materials can be manipulated through the application of magnetic forces. They have been extensively scrutinized and broadly applied in an assortment of engineering scenarios, as documented by Rosensweig in [26]. Moatimid and El-Dib [19] undertook an exploration into the stability of an interface delineating two unyielding magnetic fluids characterized by distinct densities. These fluids flowed in parallel orientation, influenced by an oblique magnetic field. Elhefnawy [8] further enriched this domain by addressing the nonlinear stability exhibited by ferromagnetic fluids. Anjali Devi and Hemamalini [6] delved into the ramifications of a normal magnetic field on RTI manifesting within rotating layers of fluid. The fluids under consideration possessed negligible viscosity and the investigation of stability encompassed nonlinear analyses. Moatimid [18] probed the stability attributes of two magnetically fluidized columns undergoing rigid rotation within an environment of zero gravity. The collective insights from these inquiries substantially augment our comprehension of the intricate dynamics underpinning the stability of magnetic fluids across diverse contextual settings. Shukla and Awasthi [28] systematically investigated the effects stemming from a vertically applied magnetic field, thereby extending the scope of exploration.

With the rapid progress of technology and the expanding range of nanofluid applications in various industrial processes, numerous researchers have dedicated efforts to explore instabilities arising from the mixing of different nanofluids under diverse conditions and configurations. In [11], He and Elazem conducted a study on the impact of radiation on the flow of nanofluids containing carbon nano-tubes in the presence of a magnetic field, specifically around a stretched sheet experiencing slip conditions. The implications of their findings extend to various domains, including thermo-mechanical processes, biomedical applications, and the design of efficient heat transfer systems for renewable power generation. This research holds promise for advancing technologies and processes in these fields by enhancing our understanding of fluid dynamics and heat transfer in complex systems influenced by radiation and magnetic fields. He et al. [13] explored the characteristics of a non-Newtonian MHD Carreau nanofluid flowing over a vertically stretched cylinder within an incompressible boundary layer. The unique aspect of this study involves the presence of mobile microorganisms and the flow occurs through permeable media, adhering to the modified Darcy's law.

In [16], Kumar et al. conducted a study focused on optimizing micro-channel heat sinks through irreversibility analysis. The research involved employing a nanofluid consisting of Al_2O_3 -water, with varying concentrations of nanoparticles and temperature-dependent properties, as the chosen coolant. Zhang et al. [30] conducted an experimental study involving the displacement of hexadecane by a micellar nanofluid within a glass capillary. This research investigates the interplay of micellar nanofluids and hydrocarbon fluids, providing insights into displacement mechanisms and fluid behavior within confined spaces. Moatimid and Hassan [20] conducted an analysis on the linear convective stability of a viscoelastic nanofluid of Walter's type within a vertical layer. In a related study [21], Moatimid et al. discussed the linear stabil-

ity analysis of two electrically conducting nanofluid layers. Temporal instability between two nanofluids in a swirling annular layer was presented by Moatimid et al. in [22]. Moatimid and Mohamed [24] conducted an analysis focusing on the nonlinear stability of two viscoelastic electrified superimposed liquids within a porous medium. This study delves into the intricate dynamics of the interplay between viscoelastic properties, electrical influences, and the porous environment. In [23], Moatimid et al. thoroughly examined the nonlinear stability of a planar interface between two fluids characterized by Walter’s B type. The study specifically investigated the influence of a constant tangential electric field on two dielectric fluids in the presence of steady relative velocities. Agarwal et al. [1] investigated a spherical nanofluid interface and observed that the viscosity of the nanofluid contributes to interface stabilization, while the fractal index of the nanoparticles exhibits a destabilizing nature.

Nanofluids influenced by a magnetic field have diverse applications, including targeted drug delivery where magnetic nanoparticles aid in controlled drug release. In heat transfer, these nanofluids can enhance thermal conductivity, improving efficiency in cooling systems. Additionally, magnetic nanofluids play a role in hyperthermia for cancer treatment, as their response to magnetic fields can generate localized heat to target and destroy cancer cells. In this investigation, we examine the impact of a tangential magnetic field on the stability of the nanofluid interface. The mathematical equations governing the system are derived within the framework of the viscous potential flow theory. This theoretical approach takes into account the viscosity of the fluids in the analysis while considering the flow to be irrotational. At the interface, the stress balance equation considers normal viscous stresses, and their difference is counteracted by interfacial tension.

2. Mathematical formulation and boundary conditions

2.1. Mathematical model

A nanofluid layer is present above a viscous liquid, Fig. 1. The height $z = h_n$ is the thickness of the nanofluid with density ρ_n , viscosity μ_n and magnetic permeability μ_m^n . The height $z = -h_v$ is the thickness of the viscous fluid with density ρ_v , viscosity μ_v and magnetic permeability μ_m^v . The equation $z = 0$ represents interfacial equation at the equilibrium. The magnetic field intensity H is applied in the direction of the x -axis.

If $\mathbf{U}_n = (u_n, v_n)$ and $\mathbf{U}_v = (u_v, v_v)$ denote the velocities in viscous fluid and nanofluid phases, the equations that govern the upper and lower phases are [6]

$$\nabla \cdot \mathbf{U}_n = 0, \quad \rho_n \left[\frac{\partial \mathbf{U}_n}{\partial t} + (\mathbf{U}_n \cdot \nabla) \mathbf{U}_n \right] = -\nabla p_n + \mu_n \nabla^2 \mathbf{U}_n + \rho_n \mathbf{g} + \mathbf{J} \times \mathbf{H}, \quad (1)$$

$$\nabla \cdot \mathbf{U}_v = 0, \quad \rho_v \left[\frac{\partial \mathbf{U}_v}{\partial t} + (\mathbf{U}_v \cdot \nabla) \mathbf{U}_v \right] = -\nabla p_v + \mu_v \nabla^2 \mathbf{U}_v + \rho_v \mathbf{g} + \mathbf{J} \times \mathbf{H}, \quad (2)$$

where p_n and p_v stand for the pressures of the nanofluid and viscous incompressible fluid phases, respectively, \mathbf{J} denotes the current density, while \mathbf{H} is the magnetic field vector defined as $\mathbf{H} = H \hat{e}_x$.

The density ρ_n and viscosity μ_n may be represented using the subsequent expressions [1]

$$\rho_n = \phi \rho_p + (1 - \phi) \rho_f, \quad (3)$$

where ρ_f denotes the density of the base fluid, ρ_p signifies the density of the metal particles, and the nanoparticle volume fraction is indicated by ϕ . Zuo [31] has also suggested a viscosity

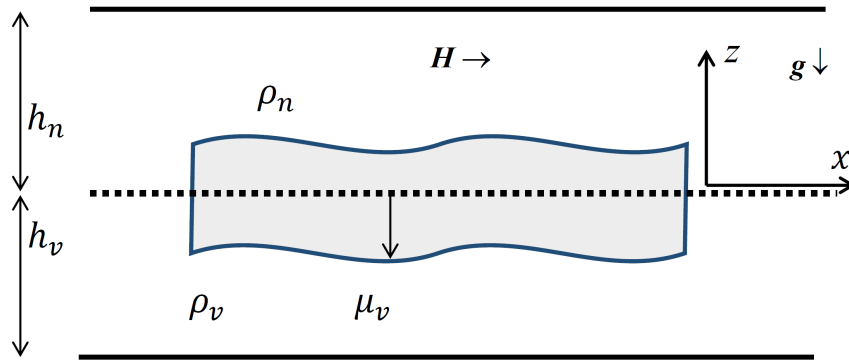


Fig. 1. Layout of the considered problem

model for the nanofluids

$$\mu_n = \mu_{ef} \left(1 - \frac{\phi_{ag}}{\phi_m} \right)^{-[\delta]\phi_m}, \quad (4)$$

where μ_{ef} stands for the viscosity of the pristine fluid, ϕ_m represents the uppermost volume fraction achievable for spheroidal nanoparticles, and the shape parameter of the nanoparticles is labeled as δ . The aggregate volume fraction of the nanoparticles, denoted as ϕ_{ag} , can be expressed using the equivalent volume fractions of the nanoparticles, denoted as ϕ_{mod} , and the fractal index d , as detailed by Agarwal et al. in [1],

$$\phi_{ag} = \phi_{mod} \left(\frac{r_a}{r} \right)^{3-d}. \quad (5)$$

In this context, the equivalent volume fractions of the nanoparticles ϕ_{mod} can be formulated in relation to the volume fraction ϕ , the interfacial layer thickness γ , and the lengths of the nanoparticles semi-minor and semi-major axes, b and a , respectively. In [10], He and Liu presented comprehensive formulas related to nanofluid flow in porous media as

$$\phi_{mod} = \phi \left(1 + \frac{\gamma}{a} \right) \left(1 + \frac{\gamma}{b} \right)^2. \quad (6)$$

2.2. Interfacial and boundary conditions

In [12], He et al. introduced a model for the flow of an electromagneto-nanofluid, exploring the dynamics of a radiative electromagnetic-Casson nanofluid flowing past a stretching sheet. Their study incorporates the influences of a chemical reaction and nonlinear thermal radiation. The continuity of the tangential magnetic field component is required at the interface [28], i.e.,

$$\mathbf{n} \times \|\mathbf{H}\| = \mathbf{0}, \quad (7)$$

where $\|x\| = x_n - x_v$.

A disparity exists in the regular current across the interface: The buildup of charge within a material element is counteracted by conduction from the surrounding fluid on both sides of the boundary. The prescribed condition at the interface, pertaining to the normal component of magnetic induction, is expressed as [28]

$$\mathbf{n} \cdot \|\mu_m \mathbf{H}\| = 0. \quad (8)$$

Additionally, the fluids will remain confined within the rigid boundaries, resulting in

$$v_n = 0 \quad \text{at } z = h_n, \quad v_v = 0 \quad \text{at } z = -h_v. \quad (9)$$

3. Stability analysis

3.1. Basic state

In its fundamental state, the interface will exist at $z = 0$ and the fluid velocities $\mathbf{U}_n(u_n, v_n) = (0, 0)$ and $\mathbf{U}_v(u_v, v_v) = (0, 0)$. Hence, the pressures will be constant and equal to c .

3.2. Perturbed state

Upon the introduction of a disturbance to the system, the equation governing the interface transforms to $z = \ell(x, t)$. As a result, the perturbed flow field can be represented as

$$\mathbf{U}_n = \mathbf{0} + \mathbf{U}'_n = (u'_n, v'_n), \quad \mathbf{U}_v = \mathbf{0} + \mathbf{U}'_v = (u'_v, v'_v), \quad p_n = c + p'_n, \quad p_v = c + p'_v.$$

The equation of magnetic field strength in the perturbed state is given as

$$\mathbf{H}_i = H\hat{e}_x - \nabla\psi_i, \quad i = n, v. \tag{10}$$

The perturbed state is characterized by the following linear equations:

$$\nabla \cdot \mathbf{U}'_n = 0, \quad \rho_n \left(\frac{\partial \mathbf{U}'_n}{\partial t} \right) = -\nabla p_n + \mu_n \nabla^2 \mathbf{U}'_n + \rho_n \mathbf{g} + \mathbf{J} \times \mathbf{H}_n, \tag{11}$$

$$\nabla \cdot \mathbf{U}'_v = 0, \quad \rho_v \left(\frac{\partial \mathbf{U}'_v}{\partial t} \right) = -\nabla p'_v + \mu_v \nabla^2 \mathbf{U}'_v + \rho_v \mathbf{g} + \mathbf{J} \times \mathbf{H}_v. \tag{12}$$

The disturbed flow is assumed to lack rotation, hence, $\mathbf{U}'_n = \nabla\phi'_n$, $\mathbf{U}'_v = \nabla\phi'_v$, where ϕ' is the velocity potential function. The fluids maintain incompressibility, implying $\nabla^2\phi'_n = 0$, $\nabla^2\phi'_v = 0$. Under these circumstances, we suppose the validity of the quasi-static approximation, allowing the computation of the magnetic field via a harmonic magnetic scalar potential function, namely $\nabla^2\psi_n = 0$, $\nabla^2\psi_v = 0$. The perturbed tangential magnetic field and perturbed normal magnetic induction can be expressed in their linear forms as follows:

$$\frac{\partial\psi_n}{\partial x} = \frac{\partial\psi_v}{\partial x}, \tag{13}$$

$$\mu_m^n \left(\frac{\partial\psi_n}{\partial z} + H \frac{\partial\ell}{\partial x} \right) = \mu_m^v \left(\frac{\partial\psi_v}{\partial z} + H \frac{\partial\ell}{\partial x} \right), \tag{14}$$

$$\frac{\partial\psi_n}{\partial x} = 0 \quad \text{at } z = h_n, \quad \frac{\partial\psi_v}{\partial x} = 0 \quad \text{at } z = -h_v. \tag{15}$$

The conditions for the velocity potential at the interface is given by

$$\frac{\partial\phi'_n}{\partial x} = \frac{\partial\ell}{\partial t} \quad \text{at } z = 0, \quad \frac{\partial\phi'_v}{\partial x} = \frac{\partial\ell}{\partial t} \quad \text{at } z = 0. \tag{16}$$

The dynamic equation governing the free surface equilibrium involves the equilibrium between the disparity in normal stresses and the surface forces acting at the free surface. The coupling of normal stresses at the interface occurs in conjunction with pressures and the normal component of viscous stresses, emphasizing the interconnected nature of these factors in the dynamics of the system. This interplay reflects the complex relationship between surface

forces and stress components at the free surface. The linear dynamical equation at the interface is given as [18, 28]

$$\left[p_n - 2\mu_{ef} \left(1 - \frac{\phi_{ag}}{\phi_m} \right)^{-[\delta]\phi_m} \frac{\partial^2 \varphi'_n}{\partial z^2} \right] - \left(p_v - 2\mu_v \frac{\partial^2 \varphi'_v}{\partial z^2} \right) + H \left(\mu_m^n \frac{\partial \psi_m^n}{\partial x} - \mu_m^v \frac{\partial \psi_m^v}{\partial x} \right) + (\rho_n - \rho_v)g = -\sigma \frac{\partial^2 \ell(x, t)}{\partial x^2}. \quad (17)$$

The normal mode procedure is utilized and the perturbed quantities are expressed as $G'(x, z, t) = \bar{G}(z)e^\eta$ and $\ell(x, t) = \ell_0 e^\eta$ with $\eta = ikx - i\omega t$, where ω is the complex frequency $\omega = \omega_R + i\omega_I$, and k denotes the wavenumber of the perturbation.

4. Dispersion relation

By employing the technique of normal mode analysis, the solution for the potential functions φ'_n and φ'_v can be determined, involving certain unspecified constants. These potential functions adhere to (9) and (16), allowing the expressions to be formulated as follows:

$$\varphi'_n = \frac{i\omega \cosh [k(z - h_n)]}{k \sinh(kh_n)} \ell_0 e^\eta, \quad \varphi'_v = -\frac{i\omega \cosh [k(z + h_v)]}{k \sinh(kh_v)} \ell_0 e^\eta. \quad (18)$$

The magnetic potential functions can be computed using the conditions (13)–(15) as

$$\psi_n = \frac{iH(\mu_m^n - \mu_m^v)}{[\mu_m^n \coth(kh_n) + \mu_m^v \coth(kh_v)]} \frac{\sinh [k(z - h_n)]}{\sinh(kh_n)} \ell_0 e^\eta, \quad (19)$$

$$\psi_v = \frac{iH(\mu_m^n - \mu_m^v)}{[\mu_m^n \coth(kh_n) + \mu_m^v \coth(kh_v)]} \frac{\sinh [k(z + h_v)]}{\sinh(kh_v)} \ell_0 e^\eta. \quad (20)$$

The pressures in (17) can be computed through the Bernoulli's equation and, hence, equation (17) takes the form as

$$\left(\rho_n \frac{\partial \varphi'_n}{\partial t} - \rho_v \frac{\partial \varphi'_v}{\partial t} \right) + 2 \left[\left(1 - \frac{\phi_{ag}}{\phi_m} \right)^{-[\delta]\phi_m} \frac{\partial^2 \varphi'_n}{\partial z^2} - \mu_v \frac{\partial^2 \varphi'_v}{\partial z^2} \right] + H_0 \left(\mu_m^n \frac{\partial \psi_m^n}{\partial x} - \mu_m^v \frac{\partial \psi_m^v}{\partial x} \right) + (\rho_n - \rho_v)g = -\sigma \frac{\partial^2 \ell(y, t)}{\partial y^2}. \quad (21)$$

By substituting the values obtained from (18)–(20) into (21), we establish the connection between the growth rate parameter and the wavenumber as described below:

$$M_2 \omega^2 + iM_1 \omega - M_0 = 0, \quad (22)$$

where

$$M_2 = \rho_n \coth(kh_n) + \rho_v \coth(kh_v),$$

$$M_1 = 2k^2 \left[\mu_{ef} \left(1 - \frac{\phi_{ag}}{\phi_m} \right)^{-[\delta]\phi_m} \coth(kh_n) + \mu_v \coth(kh_v) \right],$$

$$M_0 = \sigma k^3 - (\rho_n - \rho_v)gk + \frac{k^2 H^2 (\mu_m^n - \mu_m^v)^2}{\mu_m^n \coth(kh_n) + \mu_m^v \coth(kh_v)}.$$

Since $\omega = \omega_R + i\omega_I$, and therefore, equation (22) can be separated as

$$M_2(\omega_R^2 - \omega_I^2) - M_1\omega_I - M_0 = 0, \tag{23}$$

$$2\omega_R\omega_I M_2 + M_1\omega_R = 0 \implies \omega_R = 0. \tag{24}$$

Hence, equation (22) can be re-written as

$$M_2\omega_I^2 + M_1\omega_I + M_0 = 0. \tag{25}$$

If the upper fluid is also a viscous fluid, the expression of Joseph et al. [15] can be achieved from (25).

By employing the Routh-Hurwitz criteria to (25), the stability condition is expressed as $M_2 > 0$, $M_1 > 0$, $M_0 > 0$. The first condition ($M_2 > 0$) is evident and considering the positivity of μ_{ef} and μ_v , it follows that $M_1 > 0$. Consequently, the stability criterion dictates that $M_0 > 0$, while the condition for a marginal state is characterized by $M_0 = 0$, i.e.,

$$\sigma k^2 - (\rho_n - \rho_v)g + \frac{kH^2(\mu_m^n - \mu_m^v)^2}{\mu_m^n \coth(kh_n) + \mu_m^v \coth(kh_v)} = 0. \tag{26}$$

We found that the viscosity does not affect the stability criterion.

Introducing the characteristic velocity as well as the characteristic length, denoted as V and $h = h_n + h_v$, respectively, enables the expression of the dimensionless representation of the remaining physical parameters as follows:

$$\text{Re}_n = \frac{\rho_n h V}{\mu_{ef}}, \quad \text{We}_n = \frac{\rho_n h V^2}{\sigma}, \quad \rho = \frac{\rho_v}{\rho_n}, \quad \mu = \frac{\mu_v}{\mu_{ef}}, \quad \bar{\mu}_m = \frac{\mu_m^v}{\mu_m^n}, \quad J = \frac{\omega_I h}{V}, \quad \bar{H} = \frac{H}{V} \sqrt{\frac{\mu_m^n}{\rho_n}}.$$

The dimensionless form of (25) can be obtained as

$$\bar{L}_2 J^2 + \bar{L}_1 J + L_0 = 0, \tag{27}$$

where

$$\begin{aligned} \bar{L}_2 &= \coth(\bar{k}h_n) + \frac{1 - \text{At}}{1 + \text{At}} \coth(\bar{k}h_v), \\ \bar{L}_1 &= \frac{2\bar{k}^2}{\text{Re}_n} \left[\left(1 - \frac{\phi_{ag}}{\phi_m}\right)^{-[\delta]\phi_m} \coth(\bar{k}h_n) + \mu \coth(\bar{k}h_v) \right], \\ \bar{L}_0 &= -\frac{2\text{At}}{1 + \text{At}} \frac{\bar{k}}{\text{Fr}^2} + \frac{\bar{k}^3}{\text{We}_v} - \frac{\bar{k}^2 \bar{H}^2 (1 - \bar{\mu}_m)^2}{\coth(\bar{k}h_n) + \bar{\mu}_m \coth(\bar{k}h_v)}. \end{aligned}$$

5. Results and discussions

In this section, we expound upon the computational procedures applied to the considered model, utilizing equation (27), which characterizes a second-order algebraic equation. Upon solving this equation for a defined set of inputs, two distinct values of the growth rate J emerge. In this analysis, the larger of the two values is plotted to symbolize the growth rate in our visualization, providing insights into the model behavior under specific conditions. The following set of values are considered for the numerical computation:

$$\bar{h}_n = 0.3, \quad \text{At} = 0.8, \quad \text{Re}_n = 50, \quad \text{We}_n = 1.7, \quad \text{Fr} = 1.3, \quad \bar{H} = 2.0, \quad \bar{\mu}_m = 0.6.$$

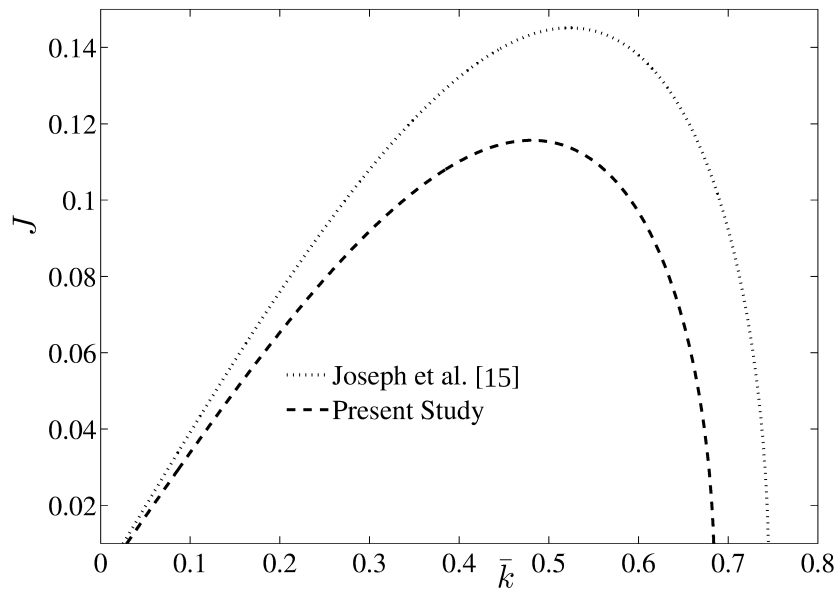


Fig. 2. Comparison with existing results

In [15], Joseph et al. investigated the interface of a viscous-viscous fluid using the irrotational theory of viscous fluids, with a focus on a channel flow with a top-heavy configuration. In contrast, our current study considers the upper fluid as nanofluid and the presence of a magnetic field. Fig. 2 presents a comparison between the growth rates observed by Joseph et al. in [15] and our results. It is crucial to highlight that in the presence of a magnetic field, perturbations exhibit a slower growth rate compared to scenarios without a magnetic field. This disparity indicates that the magnetic field introduces a stabilizing influence. Considering the magnetic field in our study, there is a notable increase in the Lorentz force within the fluid phases, opposing the movement of disturbances and contributing to the observed stabilization effect.

The graphical representation in Fig. 3 illustrates the stability growth curves attained under varying Atwood numbers. The curves corresponding to the growth rate J are depicted alongside the wavenumber \bar{k} . Clearly, this illustration demonstrates higher growth as the Atwood number increases. Thus, these dimensionless parameters play a role in initiating instability in the nanofluid interface.

The Atwood number, $At = (\rho_n - \rho_v) / (\rho_n + \rho_v)$, which is defined as the ratio of viscous fluid density ρ_v to the density of the nanofluid ρ_n , becomes a pivotal factor. With ρ_v held constant and ρ_n increased, the resultant escalation of inertial forces induces a commensurate augmentation in the growth of interface disturbances. Thus, an augmentation in nanofluid density precipitates an unstable interface. The rise in inertial forces attributable to the heightened nanofluid density exerts a discernible impact on the interface. This impetus induces acceleration in interfacial disturbances, thereby engendering a deferment in the attainment of stability.

Fig. 4 portrays the growth curves corresponding to diverse non-dimensional Froude numbers (Fr). These curves conspicuously illustrate an expanding stable domain as the Froude number is increased. Consequently, it can be postulated that the Froude number exerts a stabilizing influence on the interface by mitigating disturbance growth. The non-dimensional Froude number is predicated on the ratio of inertial force to gravitational force. It serves as a metric to analyze the interplay between gravitational acceleration and inertial forces. Notably, this parameter offers insight into the manner in which gravitational acceleration modulates inertial forces.

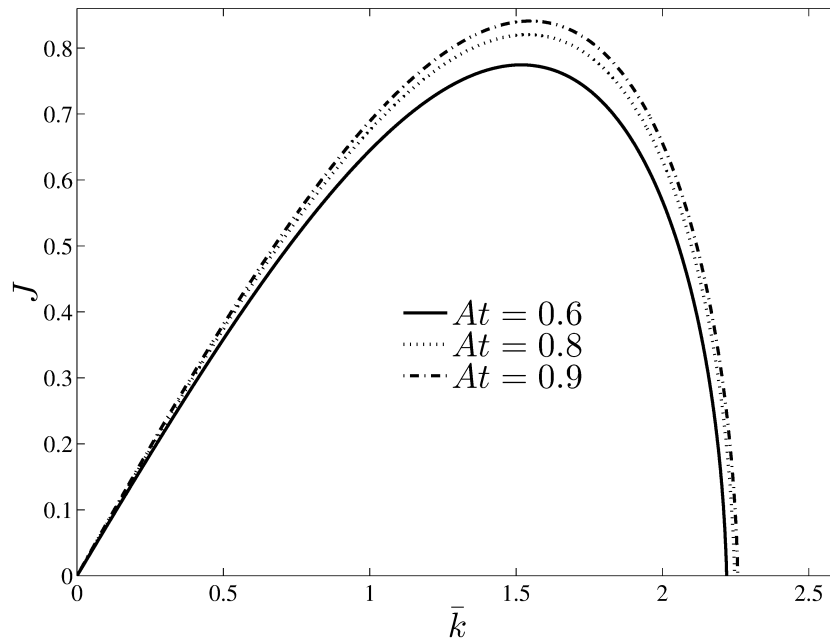


Fig. 3. Effect of the Atwood number

In Fig. 5, a comprehensive illustration is presented, elucidating the impact of magnetic field strength \bar{H} on the interface of the viscoelastic fluid. Notably, as the intensity of the magnetic field \bar{H} is heightened, a concomitant increase in perturbation growth becomes evident. This phenomenon underscores the stabilizing role of the magnetic field on the nanofluid-viscous fluid interface. This stabilization phenomenon is attributed to the emergence of the Lorentz force, engendered by perturbations in both velocity and magnetic fields. This counteracting force hampers the motion of the interface, effectively impeding the propagation of disturbances at their intrinsic pace. Hence, the velocity of disturbances diminishes, compelling the interface

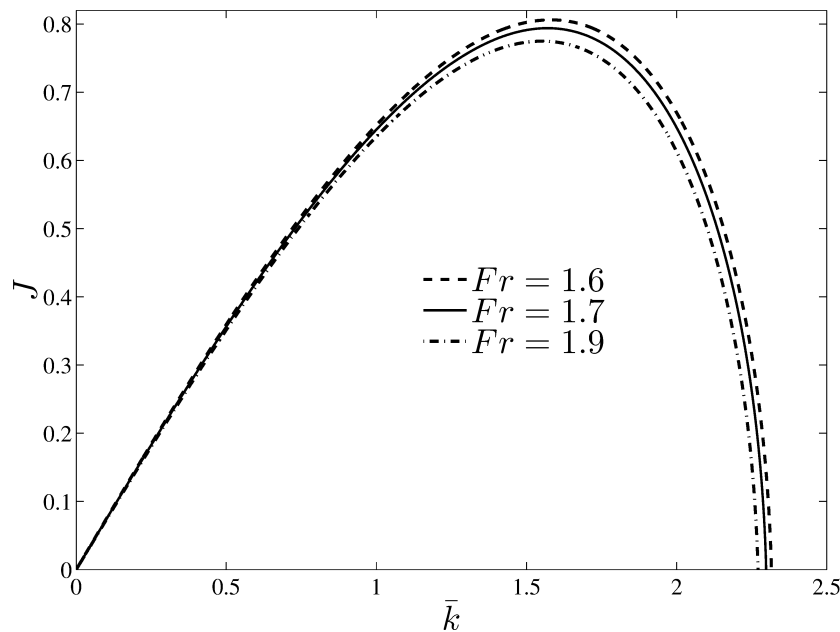


Fig. 4. Effect of the Froude number

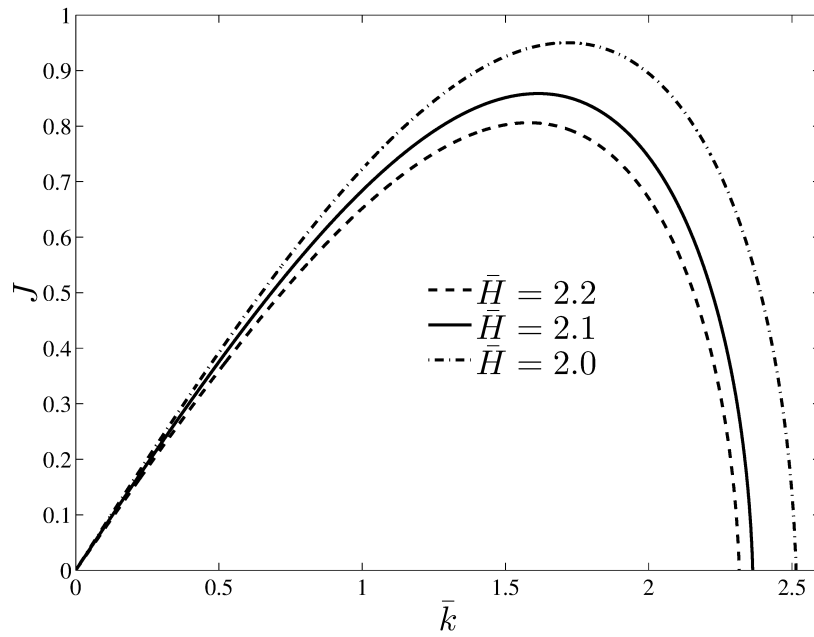


Fig. 5. Effect of magnetic field strength

to transition towards a state of stability.

Fig. 6 illustrates growth curves depicting the influence of varying nanofluid thicknesses h_n on the interface. Notably, a discernible trend emerges, wherein higher thicknesses of the nanofluid result in augmented perturbation growth. This trend signifies that the thickness of the nanofluid layer contributes to the initiation of instability within the interface. The augmenting nanofluid thickness leads to an elevation in gravitational acceleration. Therefore, this intensified gravitational force accelerates the interface in a downward direction, culminating in the destabilization of the system. Therefore, the thickness of the nanofluid layer exerts a notable destabilizing impact on the interface.

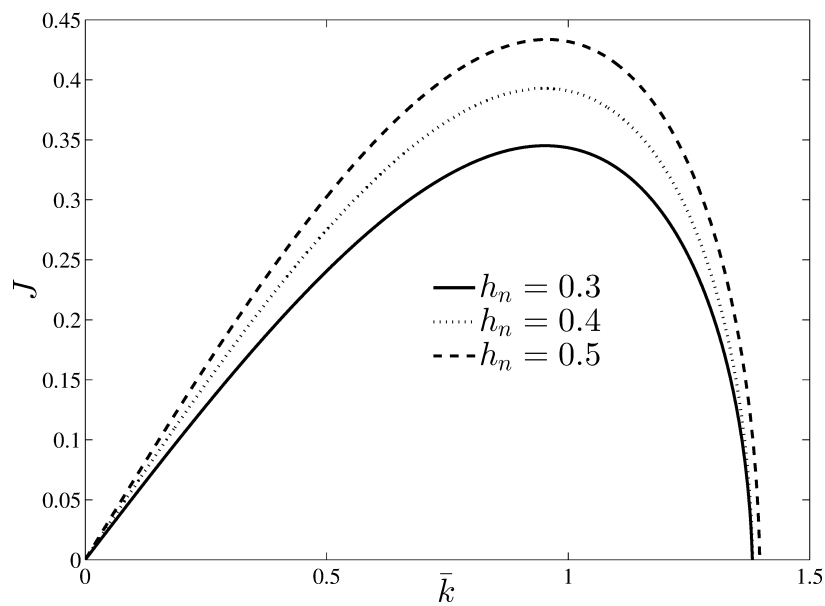


Fig. 6. Effect of nanofluid thickness

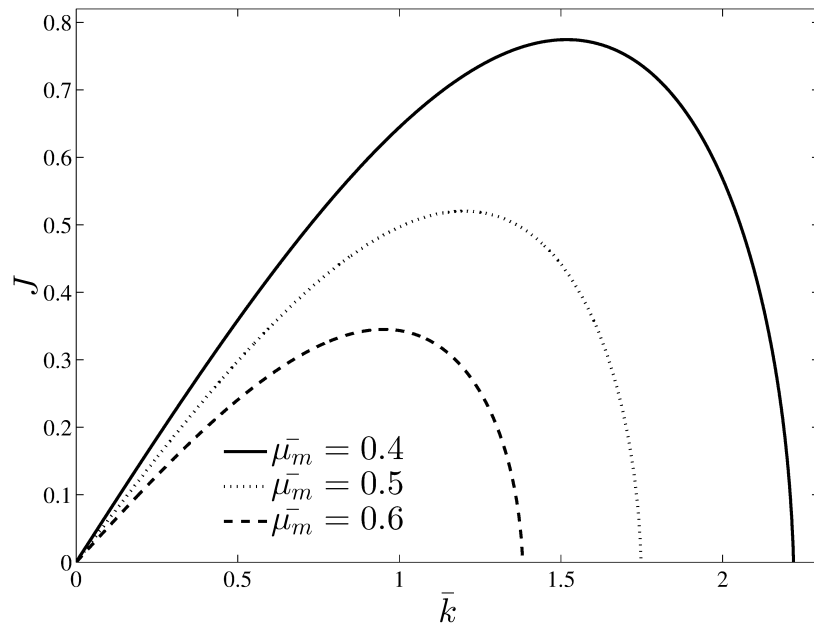


Fig. 7. Effect of magnetic induction

Fig. 7 shows the variation of the growth rate J across diverse magnetic permeability ratio values $\bar{\mu}_m$ for a specific magnetic field intensity $\bar{H} = 2$ and volume fraction $\phi = 0.05$. Evidently, the depicted trend unveils an initial augmentation in the growth of disturbance waves as the ratio of magnetic permeability between the two fluids increases, followed by a subsequent decline. This progression indicates that the magnetic permeability ratio $\bar{\mu}_m$ exhibits a stabilizing nature in the context of the stability analysis.

In Fig. 8, growth curves are plotted to elucidate the impact of the non-dimensional Reynolds number (Re_n). An elevation in the Reynolds number correspondingly yields an augmentation in the growth curves. This phenomenon underscores a context, wherein disturbance growth

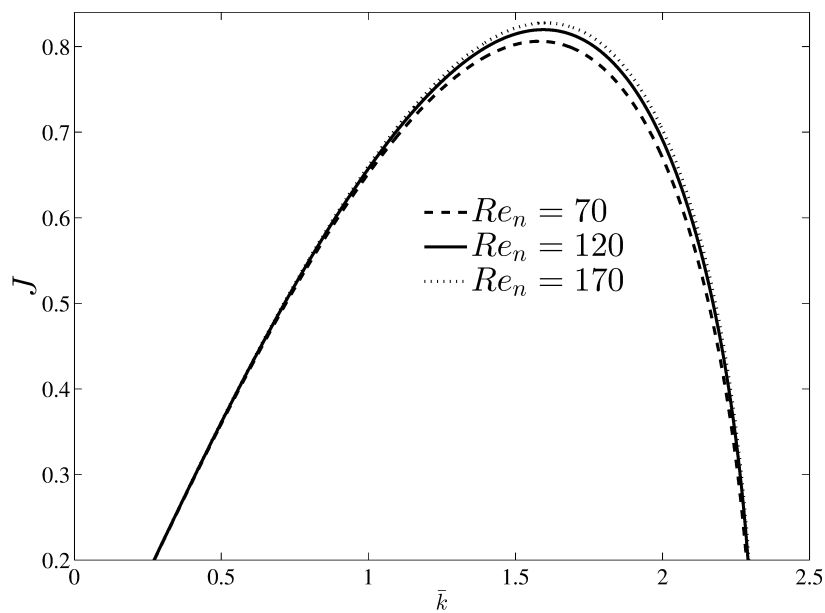


Fig. 8. Effect of the Reynolds number

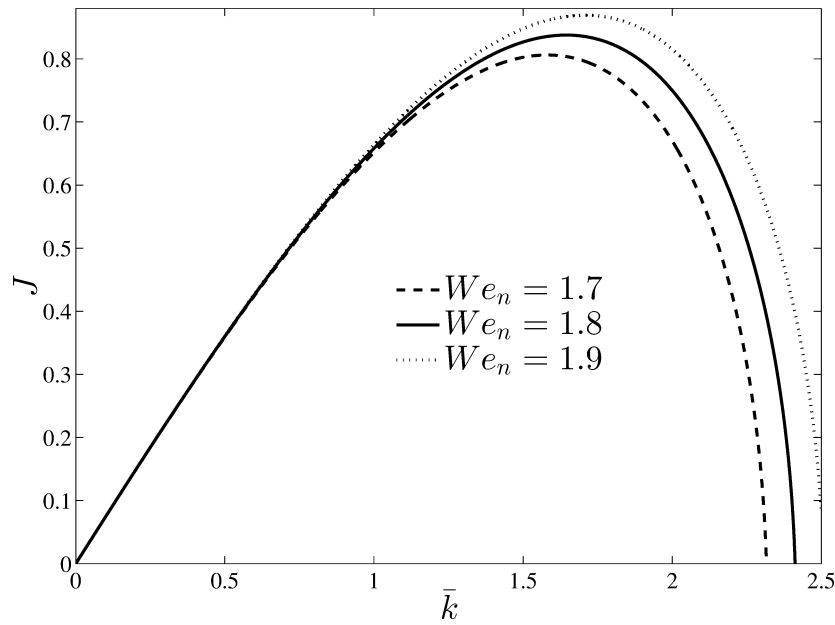


Fig. 9. Effect of the Weber number

escalates at the interface of the nanofluid. The non-dimensional Reynolds number Re_n is fundamentally indicative of the ratio of inertial to viscous forces, designated as $Re_n \propto \rho_n$ and $Re_n \propto 1/\mu_n$, respectively. This distinction imparts significant influence on perturbation growth. Notably, the augmentation of the nanofluid density ρ_n contributes to the amplification of the perturbation growth, driven by heightened inertial forces. Therefore, an intensified gravitational pull ensues due to increased density in the upper fluid, leading to a more pronounced downward force on the interface. This cascade of effects culminates in interface destabilization. Conversely, an elevation in the nanofluid viscosity μ_n operates in an opposing manner, dampening the surge in disturbances. This is attributed to the resistive nature of fluids with elevated viscosity. As a result, the interface is imbued with heightened stability, as the increased viscosity inherently curtails the escalation of disturbances.

Within Fig. 9, a graphical representation unfolds, wherein the non-dimensional wavenumber is charted across discrete values of the Weber number (We_n). Notably, the visual representation delineates an augmentation in the growth curves corresponding to increasing Weber numbers, indicative of a destabilizing tendency attributed to the Weber number. The Weber number, established as the ratio of inertial to surface forces $We_n \propto \rho_n/\sigma$, holds significance in this context. Evidently, surface tension emerges as a pivotal factor, exerting a stabilizing impact due to its reciprocal relationship with the Weber number. This interdependence stems from the fact that higher surface tension entails a stronger influence of intermolecular cohesive forces. Consequently, this enhanced cohesion mitigates disturbance growth, ultimately fostering the stabilization of the nanofluid interface.

6. Conclusions

The investigation has been performed to the analysis of perturbation growth at the interface of a nanofluid with a viscous nature, subjected to a tangential magnetic field. The analytical framework rests upon the principles of the viscous irrotational flow theory, employing the normal mode procedure. A dispersion relation is deduced in terms of the perturbation growth rate and

subsequently scrutinized. The density of the nanofluid serves to disrupt the interface stability, while the stabilizing influence exhibited by the density of the viscous fluid. The interplay of surface tension and nanofluid viscosity steers the interface towards a state of stability, whereas the viscosity inherent to the lower fluid engenders an opposing destabilizing effect. Additionally, the interface thickness of the nanofluid is observed to impose a propensity towards destabilization upon the perturbation growth of the interface. Further findings elucidate the favorable impact of the magnetic field strength on the interface stabilization, while the magnetic permeability similarly exerts a stabilizing influence on the interface dynamics.

References

- [1] Agarwal, S., Awasthi, M. K., Shukla, A. K., Stability analysis of water-alumina nanofluid film at the spherical interface, *Proceedings of the Institution of Mechanical Engineers, Part E: Journal of Process Mechanical Engineering* (2023). (in press) <https://doi.org/10.1177/09544089221150733>
- [2] Boffetta, G., Mazzino, A., Musacchio, S., Vozella, L., Kolmogorov scaling and intermittency in Rayleigh-Taylor turbulence, *Physical Review E* 79 (2009) No. 065301. <https://doi.org/10.1103/PhysRevE.79.065301>
- [3] Chen, C.-Y., Cheng, Z.-Y., An experimental study on Rosensweig instability of a ferrofluid droplet, *Physics of Fluids* 20 (5) (2008) No. 054105. <https://doi.org/10.1063/1.2929372>
- [4] Chen, C.-Y., Li, C.-S., Ordered microdroplet formations of thin ferrofluid layer breakups, *Physics of Fluids* 22 (1) (2010) No. 014105. <https://doi.org/10.1063/1.3298761>
- [5] Cole, R. L., Tankin, R. S., Experimental study of Taylor instability, *Physics of Fluids* 16 (11) (1973) 1810–1815. <https://doi.org/10.1063/1.1694217>
- [6] Devi, S. P. A., Hemamalini, P. T., Nonlinear Rayleigh-Taylor instability of two superposed magnetic fluids under parallel rotation and a normal magnetic field, *Journal of Magnetism and Magnetic Materials* 314 (2) (2007) 135–139. <https://doi.org/10.1016/j.jmmm.2006.12.024>
- [7] Dickstein, A. J., Erramilli, S., Goldstein, R. E., Jackson, D. P., Langer, S. A., Labyrinthine pattern formation in magnetic fluids, *Science* 261 (5124) (1993) 1012–1015. <https://doi.org/10.1126/science.261.5124.1012>
- [8] Elhefnawy, A. R. F., The nonlinear stability of mass and heat transfer in magnetic fluids, *Journal of Applied Mathematics and Mechanics* 77 (1) (1997) 19–31. <https://doi.org/10.1002/zamm.19970770104>
- [9] Emmons, H. W., Chang, C. T., Watson, B. C., Taylor instability of finite surface waves, *Journal of Fluid Mechanics* 7 (2) (1960) 177–193. <https://doi.org/10.1017/S0022112060001420>
- [10] He, C.-H., Liu, C. Fractal dimensions of a porous concrete and its effect on the concrete's strength, *Facta Universitatis – Series: Mechanical Engineering* 21 (1) (2023) 137–150. <https://doi.org/10.22190/FUME221215005H>
- [11] He, J.-H., Elazem, N. Y. A., The carbon nanotube-embedded boundary layer theory for energy harvesting, *Facta Universitatis – Series: Mechanical Engineering* 20 (2) (2022) 211–235. <https://doi.org/10.22190/FUME220221011H>
- [12] He, J.-H., Elgazery, N. S., Elagamy, K., Elazem, N. Y. A., Efficacy of a modulated viscosity-dependent temperature/nanoparticles concentration parameter on a nonlinear radiative electromagneto-nanofluid flow along an elongated stretching sheet, *Journal of Applied and Computational Mechanics* 9 (3) (2023) 848–860. <https://doi.org/10.22055/jacm.2023.42294.3905>
- [13] He, J.-H., Moatimid, G. M., Mohamed, M. A. A., Elagamy, K. A., A stretching cylindrical Carreau nanofluid border layer movement with motile microorganisms and variable thermal characteristics, *International Journal of Modern Physics B* (2023). (in press) <https://doi.org/10.1142/S0217979224502230>

- [14] Jacobs, J. W., Catton, I., Three-dimensional Rayleigh-Taylor instability – Part 1: Weakly nonlinear theory, *Journal of Fluid Mechanics* 187 (1988) 329–352.
<https://doi.org/10.1017/S002211208800045X>
- [15] Joseph, D. D., Belanger, J., Beavers, G. S., Breakup of a liquid drop suddenly exposed to a high-speed airstream, *International Journal of Multiphase Flow* 25 (6–7) (1999) 1 263–1 303.
[https://doi.org/10.1016/S0301-9322\(99\)00043-9](https://doi.org/10.1016/S0301-9322(99)00043-9)
- [16] Kumar, K., Chauhan, P. R., Kumar, R., Bharj, R. S., Irreversibility analysis in Al₂O₃-water nanofluid flow with variable property, *Facta Universitatis – Series: Mechanical Engineering* 20 (3) (2022) 503–518. <https://doi.org/10.22190/FUME210308050K>
- [17] Lewis, D. J., The instability of liquid surface when accelerated in a direction perpendicular to their planes–II, *Proceedings of the Royal Society A* 202 (1068) (1950) 81–96.
<https://doi.org/10.1098/rspa.1950.0086>
- [18] Moatimid, G. M., On the stability of two rigidly rotating magnetic fluid columns in zero gravity in the presence of mass and heat transfer, *Journal of Colloid and Interface Science* 250 (1) (2002) 108–120. <https://doi.org/10.1006/jcis.2002.8291>
- [19] Moatimid, G. M., El-Dib, Y. O., Kelvin-Helmholtz instability of miscible ferrofluids, *International Journal of Theoretical Physics* 35 (1996) 425–443. <https://doi.org/10.1007/BF02083825>
- [20] Moatimid, G. M., Hassan, M. A., Convection instability of non-Newtonian Walter’s nanofluid along a vertical layer, *Journal of the Egyptian Mathematical Society* 25 (2) (2017) 220–229.
<https://doi.org/10.1016/j.joems.2016.09.001>
- [21] Moatimid, G. M., Hassan, M. A., Linear instability of water-oil electrohydrodynamic nanofluid layers: Analytical and numerical study, *Journal of Computational and Theoretical Nanoscience* 15 (5) (2018) 1 495–1 510. <https://doi.org/10.1166/jctn.2018.7383>
- [22] Moatimid, G. M., Hassan, M. A., Mohamed, M. A. A., Temporal instability of a confined nanoliquid film with the Marangoni convection effect: Viscous potential theory, *Microsystem Technologies* 26 (2020) 2 123–2 136. <https://doi.org/10.1007/s00542-020-04772-2>
- [23] Moatimid, G. M., Mohamed, M. A. A., Elagamy, K., Nonlinear Kelvin-Helmholtz instability of a horizontal interface separating two electrified Walters’ B liquids: A new approach, *Chinese Journal of Physics* 85 (2023) 629–648. <https://doi.org/10.1016/j.cjph.2023.06.020>
- [24] Moatimid, G. M., Mohamed, Y. M., A novel methodology in analyzing nonlinear stability of two electrified viscoelastic liquids, *Chinese Journal of Physics* (2023). (in press)
<https://doi.org/10.1016/j.cjph.2023.12.030>
- [25] Rayleigh, L., *Scientific papers*, vol. 2, Cambridge, Cambridge University Press, 1890, pp. 200–207.
- [26] Rosensweig, R. E., Magnetic fluids, *Annual Review of Fluid Mechanics* 19 (1987) 437–463.
<https://doi.org/10.1146/annurev.fl.19.010187.002253>
- [27] Sharp, D. H., An overview of Rayleigh-Taylor instability, *Physica D: Nonlinear Phenomena* 12 (1–3) (1984) 3–18. [https://doi.org/10.1016/0167-2789\(84\)90510-4](https://doi.org/10.1016/0167-2789(84)90510-4)
- [28] Shukla, A. K., Awasthi, M. K., Rayleigh-Taylor instability with vertical magnetic field and heat transfer, *AIP Conference Proceedings* 2352 (1) (2021) No. 020013.
<https://doi.org/10.1063/5.0052998>
- [29] Taylor, G. I., The instability of liquid surfaces when accelerated in a direction perpendicular to their planes–I, *Proceedings of the Royal Society A* 201 (1065) (1950) 192–196.
<https://doi.org/10.1098/rspa.1950.0052>
- [30] Zhang, H., Nikolov, A., Wasan, D., Dewetting film dynamics inside a capillary using a micellar nanofluid, *Langmuir* 30–31 (2014) 9 430–9 435. <https://doi.org/10.1021/la502387j>
- [31] Zuo, Y., Effect of SiC particles on viscosity of 3-D print paste: A fractal rheological model and experimental verification, *Thermal Science* 25 (3) (2021) 2 405–2 409.
<https://doi.org/10.2298/TSCI200710131Z>